18th World Conference on Nondestructive Testing, 16-20 April 2012, Durban, South Africa

Numerical Characterisation of Guided Wave Scattering Due to Welds in Rails

Craig S. LONG, Philip W. LOVEDAY
CSIR Materials Science and Manufacturing; Pretoria, South Africa
Phone: +27 12 841 2498, Fax +27 12 841 3895; e-mail: Clong@csir.co.za, PLoveday@csir.co.za

Abstract
The analysis of travelling waves in elastic waveguides with complex cross-sections, such as train rails, can only conveniently be performed numerically. The semi-analytical finite element (SAFE) method has become a popular tool for performing such analyses. This paper employs a hybrid SAFE-3D method to investigate the scattering of guided waves interacting with discontinuities, such as welds, in continuous welded train rails. The aim of the analysis is to predict transmission and reflection coefficients for a given incident wave and known discontinuity parameters. This characterisation is useful for predicting the long-range transmission characteristics of transducers in NDT and monitoring systems, such as the rail break alarm system developed by the Institute for Maritime Technology (IMT) and the Council for Scientific and Industrial Research (CSIR). The numerical model can also be used to estimate welded sections properties from experimental measurements using a scanning laser vibrometer.

Keywords: Guided wave, train rail, scattering, weld, semi-analytical finite element (SAFE)

1. Introduction

Guided wave inspection and monitoring of structures is being researched for various industrial applications. One important application is that of rail condition monitoring where long lengths of rail can be monitored from permanently attached transducers [1].

Wave propagation in waveguides with arbitrary cross-section can be very complex, and numerical modelling is often required to predict this behaviour. The authors have recently developed modelling techniques for combining traditional 3D finite element (FE) models of transducers with 2D semi-analytical finite element (SAFE) models of waveguides [2-4]. These models are useful when designing transducers that effectively transmit a particular mode of propagation. SAFE models have also been used in conjunction with laser vibrometer measurements taken over a length of rail to identify modes of propagation [4]. All of these efforts have been aimed at designing transducers which will produce guided waves that will travel long distances.

In order to further investigate the effect of propagation over long distances, the effects of discontinuities, including welds in rails is required. Figure 1(a) depicts an example of a poor weld, while a step change in rail profile resulting from the connection of a new rail to an older rail, which has been regularly ground as part of a maintenance routine, is depicted in Figure 1(b). Furthermore, for shorter distance investigations including lab and field measurements, the interaction of waves with free ends or anchors could be required. Ideally, in future the ability to identify, characterise and locate damage to a rail is naturally also of interest (see Figure 2(b) for example). A general tool to analyse these various conditions is therefore required. This paper will detail the authors' early attempts at developing this analysis competence.

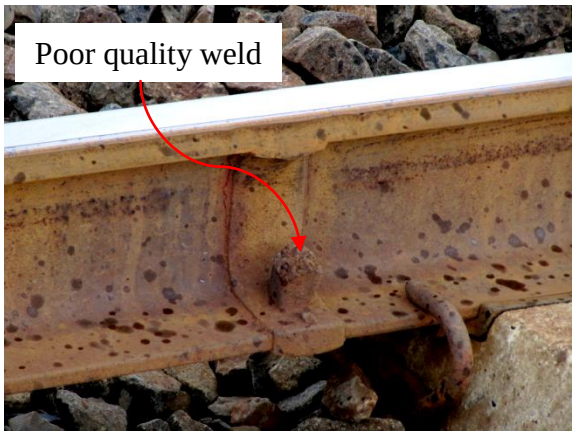

(a) Example of a poor quality weld.

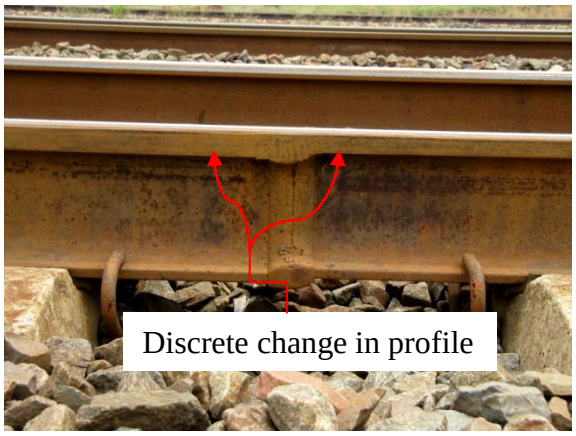

(b) Example of a step change in rail profile resulting from a connection between new and worn rail.

Figure 1. Examples of possible sources of scattering for propagating waves in rails.

Various authors have investigated the problem of analysing the interaction of propagating elastic waves with damage in infinite or semi-infinite waveguides. One technique is to employ a standard 3D FE analysis [5,6]. The advantage of this method is that commercially available FE software can be used and therefore complex shapes of waveguide cross-section and damage can easily be handled. Disadvantages include the fact that computational times and storage requirements may be extreme, especially for long waveguides at high frequencies, since wavelengths become small and fine meshes are therefore required. Furthermore, significant post-processing could be required to identify modes of propagation.

A second option is to use only semi-analytical finite elements in the analysis [7]. The advantage of this approach is that it is not usually very numerically expensive, and separation of modal information is usually quite straightforward. This approach has the problem, however, that general defects (with complex geometry) are not easy to accommodate.

Recently several authors have developed "hybrid" techniques, combining 2D SAFE models of the semi-infinite waveguide and a 3D solid FE model of the defect only [8-10]. These methods combine the salient features of the two methods mentioned above, a full 3D model of the area around the defect is required (allowing for complex geometries, but reducing computational effort) while modelling the semi-infinite waveguides using a SAFE model. In this paper, we use the implementation suggested by Benmeddour et al. [9] to study the effects discrete changes in waveguide geometry or material. The problem considered is schematically depicted in Figure 2.

2. Finite element formulation

In this section, a brief description of the numerical modelling techniques employed will be presented. The implementation is based closely on the hybrid method proposed by Benmeddour et al. [9], and will therefore not be presented in detail here. We will however, present only the salient points of their development and the same notation as in their paper will be used. The technique calls for both a semi-analytical finite element (SAFE) and a solid 3-D finite element (FE) implementation.

The SAFE element formulation used in this study is relatively well known, and is based on the implementation of Hayashi et al. [11]; their formulation will therefore not be presented at

all herein. The solid 3-D finite elements are standard displacement based elements, and more detail about their formulation can be found in, for example, Cook et al. [12].

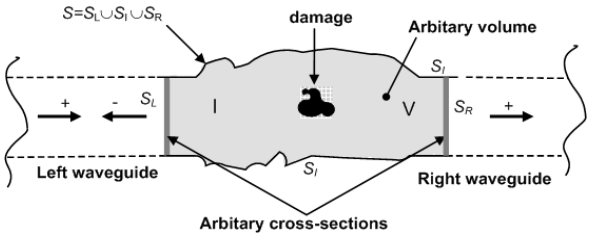

(a) Schematic of arbitrary problem under investigation. Reproduction of image from Benmeddour et al. [9].

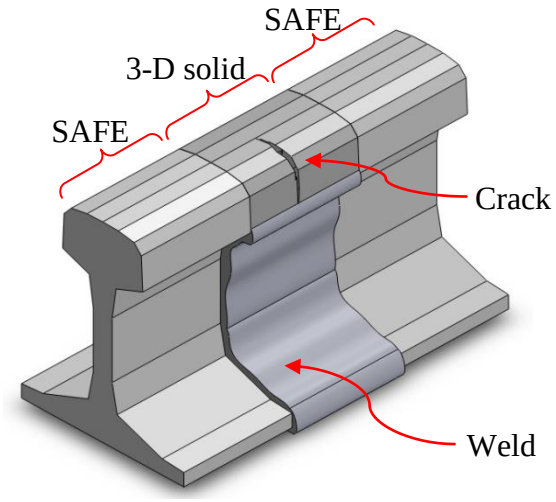

(b) Illustration of typical rail-specific applications.

Figure 2. Illustration of semi-infinite waveguides connected to a damaged volume.

A partitioned variational statement is developed by Benmeddour et al. [9] in which the displacements of the arbitrary volume depicted in Figure 2(a) are divided into degrees of freedom in contact with the left waveguide, denoted *L*, with the right waveguide, *R*, and the remaining degrees of freedom in the interior of the volume, *I*

$$\begin{Bmatrix} \delta\mathbf{U}_L \\ \delta\mathbf{U}_I \\ \delta\mathbf{U}_R \end{Bmatrix}^T \begin{bmatrix} \mathbf{D}_{LL} & \mathbf{D}_{LI} & \mathbf{D}_{LR} \\ \mathbf{D}_{IL} & \mathbf{D}_{II} & \mathbf{D}_{IR} \\ \mathbf{D}_{RL} & \mathbf{D}_{RI} & \mathbf{D}_{RR} \end{bmatrix} \begin{Bmatrix} \mathbf{U}_L \\ \mathbf{U}_I \\ \mathbf{U}_R \end{Bmatrix} - \begin{Bmatrix} \delta\mathbf{U}_L \\ \delta\mathbf{U}_I \\ \delta\mathbf{U}_R \end{Bmatrix}^T \begin{Bmatrix} \mathbf{f}_L \\ \mathbf{0} \\ \mathbf{f}_R \end{Bmatrix} = 0, \tag{1}$$

where $\mathbf{U}$ denotes the vector of nodal displacements, and $\mathbf{D}_{ij}=\mathbf{K}_{ij} - \omega^2\mathbf{M}_{ij}$ represents the dynamic stiffness matrix with $\mathbf{K}$ and $\mathbf{M}$ being the stiffness and mass matrices, respectively. The forces associated with the left and right boundaries, denoted $\mathbf{f}_L$ and $\mathbf{f}_R$, as well as the displacements in the left and right boundaries, $\mathbf{U}_L$ and $\mathbf{U}_R$, are expanded as:

$$\begin{aligned} \mathbf{U}_L &= \mathbf{B}_L^+\boldsymbol{\alpha}_L^+ + \mathbf{B}_L^-\boldsymbol{\alpha}_L^-, \quad \mathbf{U}_R = \mathbf{B}_R^+\boldsymbol{\alpha}_R^+, \\ \mathbf{f}_L &= \mathbf{T}_L^+\boldsymbol{\alpha}_L^+ + \mathbf{T}_L^-\boldsymbol{\alpha}_L^-, \quad \mathbf{f}_R = \mathbf{T}_R^+\boldsymbol{\alpha}_R^+, \quad \text{and} \\ \delta\mathbf{U}_L &= \delta\boldsymbol{\alpha}_L^{-T}\mathbf{B}_L^{-T}, \quad \delta\mathbf{U}_R = \delta\boldsymbol{\alpha}_R^{+T}\mathbf{B}_R^{+T}. \end{aligned} \tag{2}$$

In these equations, $\mathbf{B}$ and $\mathbf{T}$ represents the set of displacement and force modes respectively, and $\boldsymbol{\alpha}$ represents the vector of modal amplitudes calculated from a SAFE eigenvalue analysis and some post-processing to compute $\mathbf{T}$. As before the subscripts *L* and *R* denote the left and right waveguides and the + and – superscripts denote forward and backward propagating modes. The direction of propagation is identified based on the sign of the group velocity for real wavenumbers, and the sign of the imaginary part of the wavenumber for evanescent modes. After substitution of (2) into (1), the following linear system results:

$$\begin{bmatrix} \mathbf{B}_L^{-T} & \mathbf{0} & \mathbf{0} \\ \mathbf{0} & \mathbf{I} & \mathbf{0} \\ \mathbf{0} & \mathbf{0} & \mathbf{B}_R^{+T} \end{bmatrix} \left(\begin{bmatrix} \mathbf{D}_{LL} & \mathbf{D}_{LI} & \mathbf{D}_{LR} \\ \mathbf{D}_{IL} & \mathbf{D}_{II} & \mathbf{D}_{IR} \\ \mathbf{D}_{RL} & \mathbf{D}_{RI} & \mathbf{D}_{RR} \end{bmatrix} \begin{bmatrix} \mathbf{B}_L^{-} & \mathbf{0} & \mathbf{0} \\ \mathbf{0} & \mathbf{I} & \mathbf{0} \\ \mathbf{0} & \mathbf{0} & \mathbf{B}_R^{+} \end{bmatrix} - \begin{bmatrix} \mathbf{T}_L^{-} & \mathbf{0} & \mathbf{0} \\ \mathbf{0} & \mathbf{0} & \mathbf{0} \\ \mathbf{0} & \mathbf{0} & \mathbf{T}_R^{+} \end{bmatrix} \right) \begin{Bmatrix} \boldsymbol{\alpha}_L^{-} \\ \mathbf{U}_I \\ \boldsymbol{\alpha}_R^{+} \end{Bmatrix} =$$
$$- \begin{bmatrix} \mathbf{B}_L^{-T} & \mathbf{0} & \mathbf{0} \\ \mathbf{0} & \mathbf{I} & \mathbf{0} \\ \mathbf{0} & \mathbf{0} & \mathbf{B}_R^{+T} \end{bmatrix} \left(\begin{bmatrix} \mathbf{D}_{LL} & \mathbf{D}_{LI} & \mathbf{D}_{LR} \\ \mathbf{D}_{IL} & \mathbf{D}_{II} & \mathbf{D}_{IR} \\ \mathbf{D}_{RL} & \mathbf{D}_{RI} & \mathbf{D}_{RR} \end{bmatrix} \begin{bmatrix} \mathbf{B}_L^{+} \\ \mathbf{0} \\ \mathbf{0} \end{bmatrix} - \begin{bmatrix} \mathbf{T}_L^{+} \\ \mathbf{0} \\ \mathbf{0} \end{bmatrix} \right) \boldsymbol{\alpha}_L^{+}, \tag{3}$$

which can be solved for the unknown modal amplitudes of the reflection from the left face, $\boldsymbol{\alpha}_{\mathrm{L}}^{-}$, the transmitted modal amplitudes through the right surface, $\boldsymbol{\alpha}_{\mathrm{R}}^{+}$, and the displacements of the interior volume $\mathbf{U}_{\mathrm{I}}$, in terms of known incident modal amplitudes $\boldsymbol{\alpha}_{\mathrm{L}}^{+}$.

This full system of equations will be referred to as a SAFE-3D analysis since both SAFE and 3D FE components exist. As pointed out by Benmeddour, if the waveguide on the right (carrying the transmitted energy) does not exist, a simplified SAFE-3D analysis can be obtained by simply removing the third row and column from matrices and the third term from vectors in (3). Furthermore, if only the left waveguide is present, a further simplification is possible containing only SAFE terms:

$$\mathbf{B}_L^{-T} \mathbf{T}_L^{-} \boldsymbol{\alpha}_L^{-} = -\mathbf{B}_L^{-T} \mathbf{T}_L^{+} \boldsymbol{\alpha}_L^{+}. \tag{4}$$

This simplified system will be referred to as a SAFE-only analysis, and is similar to the method proposed in Taweel et al. [13]. The results of numerical studies are often presented in terms of power and not modal amplitude. Power flow through a surface is defined as

$$P = \int_S \overline{\mathbf{P}} \cdot \mathbf{n} \, \mathrm{d}S, \tag{5}$$

where $P_{\mathrm{i}} = -\sigma_{\mathrm{ij}} \, (\mathrm{d}u_{\mathrm{j}}/\mathrm{d}t)$ and the overbar denotes time averaging. It is shown by Benmeddour [9] that this reduces to

$$P_{nm} = |\alpha_n|^2 \frac{\omega}{2} \mathrm{Im}\left(\mathbf{U}_n^{*T} \mathbf{f}_n \right), \tag{6}$$

where Im(·) extracts only the imaginary part of the term in parentheses, and $(\cdot)^{*\mathrm{T}}$ indicates the complex transpose. The reflection and transmission coefficients are, respectively, computed by dividing the transmitted or reflected power by the power of the incident wave:

$$R_{mn} = \frac{P_{Ln}^{-}}{P_{Lm}^{+}}, \quad T_{mn} = \frac{P_{Rn}^{+}}{P_{Lm}^{+}}. \tag{7}$$

3. Numerical results

In this section, we present results from our numerical experiments. In all, four problems are considered, the first being the reflection from the free end of a circular waveguide. Since this problem is symmetric, only a quarter of the waveguide needs to be modelled (as shown in Figure 3(a). The second problem relates to the transmission of guided waves through a layer

with dissimilar material properties, using the same mesh as the first problem. These two problems are largely used to verify the correctness of our implementation. The third problem considers the reflection of a single propagating mode from the free end of a UIC-60 rail. This problem will be analysed over a wider range of frequencies. The FE mesh used for this study is depicted in Figure 3(b). Finally, the propagation of a single mode across a weld will be considered, with FE mesh shown in Figure 3(c). The solid FE meshes depicted in Figure 3 are generated by extruding the corresponding SAFE mesh associated with the various geometries under consideration. We use 4-noded quadrilateral SAFE elements and 8-noded solid brick elements throughout.

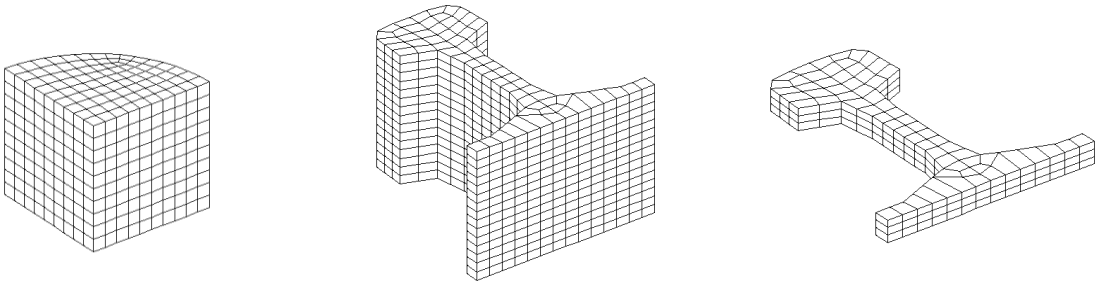

(a) Circular waveguide mesh (quarter mode).

(b) Rail mesh used to study the reflection from a free end.

(c) Rail mesh used to model propagation across a weld.

Figure 3. Solid finite element meshes used in the numerical study generated by extruding SAFE mesh in the direction of the waveguide.

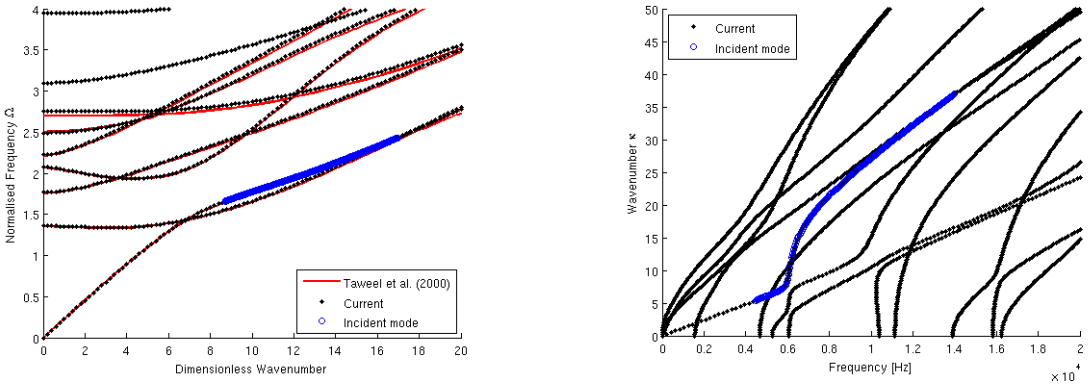

(a) Cylinder.

(b) UIC-60 rail.

Figure 4. Dispersion curves generated using a SAFE analysis

3.1 Reflection from the free end of a circular waveguide

This benchmark problem is considered in order to verify our numerical implementation. It has previously been studied by, for example Benmeddour et al. [9] as well as Taweel et al. [13]. In order to compare our results with those of previous authors, the following geometry and material properties are used. The solid waveguide radius is R=0.5 m, the length of the FE mesh depicted in Figure 3(a) is 0.5 m, the elastic modulus is E=210 GPa, while Poisson's ratio is set to ν=0.25 and mass density ρ=7800 kg/m^3.

Figure 4(a) shows our computed dispersion curves compared to those presented by Taweel et al. [13]. The normalised wavenumber, k, and frequency are computed as:

$$\Omega = \frac{\omega}{\omega_{ref}} \text{ and } k = \frac{\kappa}{R}, \text{ where} \tag{8}$$

$$\omega_{ref} = (\lambda + 2\mu)/(\rho R^2), \tag{9}$$

where λ and μ represent the Lamé constants, κ in rad/m is the wavenumber and ω is the circular frequency in rad/s. A good comparison is observed. The slight variation could be attributed to difference in SAFE discretization.

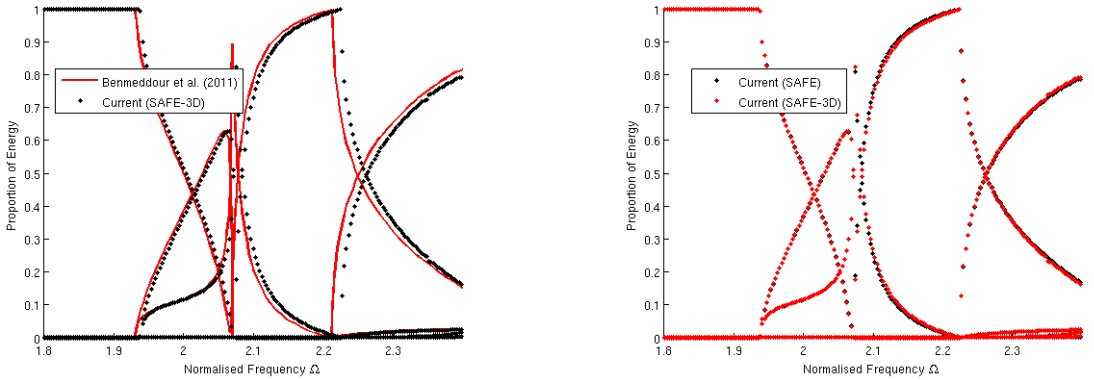

(a) Comparison with literature. (b) Comparison between SAFE-only and SAFE-3D.

Figure 5. Proportion of energy reflected from the free end of the cylinder.

Figure 5(a) presents the computed proportion of energy reflected from a traction free end with the incident mode being the first longitudinal mode (see Figure 4(a)). Results computed using a combination of SAFE and the 3D solid model are used to compare with the implementation of Benmeddour et al. [9], even though a SAFE-only model would suffice since the free end is normal to the waveguide longitudinal axis. Good agreement is achieved. The slight difference could be attributed to the fact that Benmeddour et al. use higher-order elements in their analysis.

Figure 5(b) illustrates the correspondence between the SAFE-only analysis explained in Section 2, and represented by (4) and the combination of SAFE-3D analysis represented by (3). Very good agreement is achieved at these relatively low frequencies, with a relatively fine mesh.

3.2 Transmission through a layer with dissimilar material properties

The same geometry and mesh as that used in Section 3.1 are used here. A 50% reduction in the elastic modulus is simulated (without a change in Poisson's ratio). The analytical solution for the proportion of power transmitted through the layer (T) at low frequency is given in Kinsler et al. (1982) [14] as:

$$T = \left[1 + \frac{1}{4}\left(\frac{c_2}{c_1} - \frac{c_1}{c_2} \right)^2 \sin^2(k_2 L) \right]^{-1}, \text{ where} \tag{10}$$

c_1 and c_2 are longitudinal velocities in the SAFE and the 3D solid sections respectively, and L is the layer thickness (0.5 m in this case).

Figure 6 depicts the predicted proportion of energy transmitted compared to the analytical solution over two different frequency ranges. It is clear that at low frequencies a good correspondence is achieved. Note that the minimum of the analytical solution corresponds to a frequency where a quarter of the wavelength of the longitudinal mode is equal to the layer thickness L. At higher frequencies, especially at the cut-on frequency of the next symmetric mode, the analytical solution is not valid. We also verified the trivial case where the layer has the same material, which results in 100% transmission and zero reflection, which was achieved to machine precision.

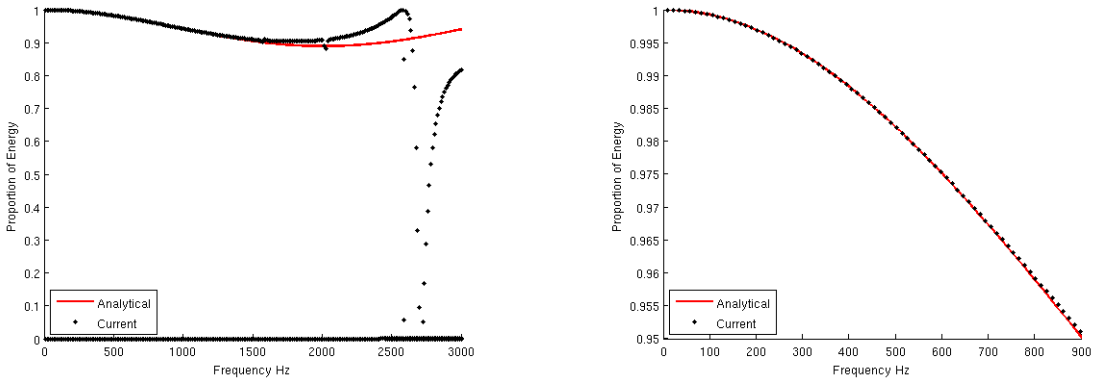

(a) Wide frequency range. (b) Narrow frequency range.

Figure 6. Proportion of energy transmitted through a layer with different material.

3.3 Reflection from the free end of a UIC-60 rail

In this section the reflection from the free end of a UIC-60 rail profile is studied. The material properties used are E=215 GPa and ν=0.3, with ρ=7800 kg/m3. The extent of the 3-D solid mesh is 100 mm. Dispersion curves with incident mode are shown in Figure 4(b).

Figures 7(a) and 7(b) show the real and imaginary parts of the incident mode shape at 4.5 kHz (see Figure 4(b) for corresponding point on the dispersion curve). Figure 7(c) shows the interior displacement ($\mathbf{U}_I$ in equation (3)) at the same frequency. Figure 7(d) presents the proportion of energy reflected by this mode over a relatively large frequency range, computed using the SAFE-only method (4), as well as the SAFE-3D solid procedure (3), presented in Section 2. The figure shows that at high frequencies, a significant difference between the SAFE-only and the SAFE-3D analysis are noted. This is presumably a result of a somewhat coarse mesh used when compared to the problem considered in Sections 3.1 and 3.2 which took advantage of the double symmetry of the geometry.

3.4 Simulation of transmission through a rail weld of dissimilar material

In this final problem, the transmission of the same incident mode considered in Section 3.3, over the same frequency range, is studied. The weld in this case extends 15 mm and has material properties arbitrarily chosen as having a 10% reduction in both elastic modulus and Poisson's ratio. In future, we will attempt to better approximate the material properties.

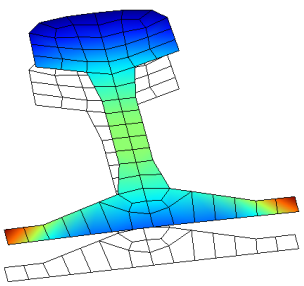

(a) Incident mode at 4.5kHz.

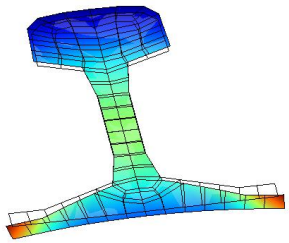

(b) Incident mode at 4.5kHz.

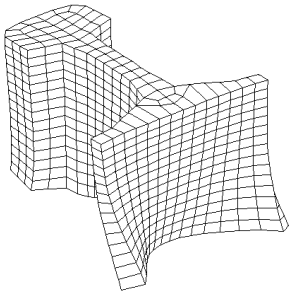

(c) Incident mode at 4.5kHz.

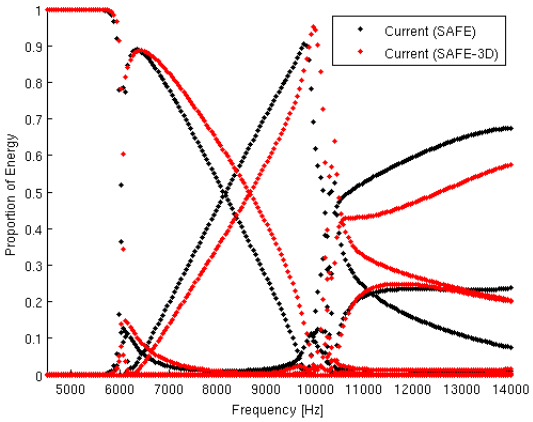

(d) Proportion of energy reflected from the free end of a rail for SAFE-only and SAFE-3D analysis.

Figure 7. Reflection from the free end of a UIC-60 rail.

Figure 8 depicts the proportion of energy which is transmitted and/or reflected. Figure 8(a) indicates a very sharp reduction in transmitted power at the cut-on frequency of the symmetric mode around 6 kHz. Figure 8(b) shows that several modes are reflected, but that their proportion of the incident power is relatively low except in the immediate vicinity of 6kHz (note that the maximum proportion of energy in Figure 8(b) is 1e-3).

Although the energy reflected at a single weld may seem fairly insignificant, the fact that transmission in the rail break alarm system needs to cover up to 1.5 km, and welds are found at approximately 20 m intervals, means that the repeated effect could be significant.

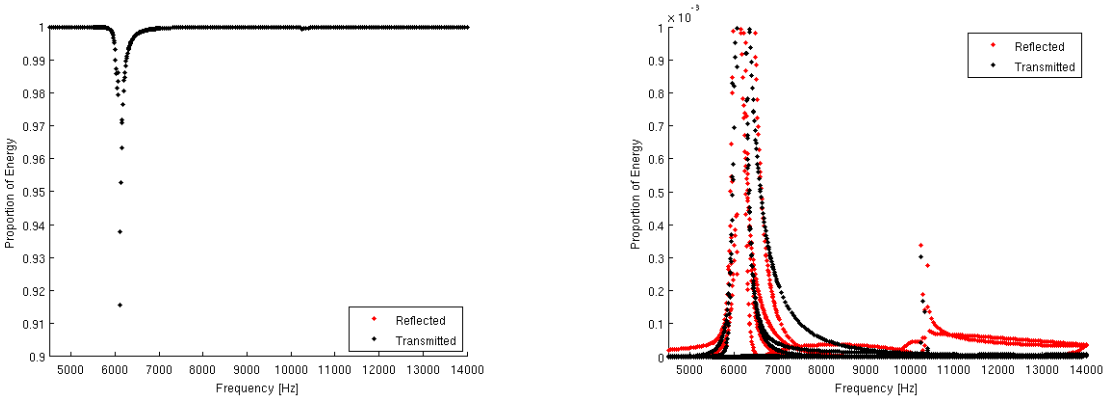

(a) (b)

Figure 8. Transmission and reflection of energy over a weld.

4. Conclusions

We have implemented a hybrid SAFE-3D finite element method [9] which, in its general form, may be used to investigate the interaction of guided waves with discrete changes in waveguide geometry and/or material properties. Benchmark examples were used to verify the correctness of our implementation, and good agreement between our computed results and previously published results were achieved. The double symmetry of the benchmark geometry was exploited, and as a result a fairly fine discretisation was employed.

We also studied the reflection of propagating waves from the free end of a rail. In this case, since symmetry was not exploited, the resulting mesh was fairly coarse. A noticeable difference between the results computed using the SAFE-only and the SAFE-3D analyses was observed, which could possibly be attributed to discretisation error. As part of a future study, a convergence study will be carried out in order to determine a suitable discretisation to solve these types of problems accurately. We also plan to implement higher-order 8-noded SAFE and 20-noded 3D solid brick elements.

Finally, the interaction of a single propagating mode with a weld in a rail was investigated. We found that although the proportion of energy which is reflected is not significant, that the additive effects over long distance could be of significance. In order to study this problem in detail, we would like to better approximate the weld material properties using scanning laser vibrometer measurements.

Acknowledgements

Financial support from the CSIR PG project number HAE012P, and the CSIR cooperation fund for scientific and technology development are gratefully acknowledged.

References

1. P. W. Loveday, “Development of piezoelectric transducers for a railway integrity monitoring system,” in *Proceedings of SPIE*, 2000, vol. 3988, pp. 330-338.
2. P. W. Loveday, “Analysis of piezoelectric ultrasonic transducers attached to waveguides using waveguide finite elements.,” *IEEE transactions on ultrasonics, ferroelectrics, and frequency control*, vol. 54, no. 10, pp. 2045 - 2051, Oct. 2007.
3. P. W. Loveday, “Simulation of piezoelectric excitation of guided waves using waveguide finite elements.,” *IEEE transactions on ultrasonics, ferroelectrics, and frequency control*, vol. 55, no. 9, pp. 2038 - 2045, Sep. 2008.
4. P. W. Loveday, “Modeling and measurement of piezoelectric ultrasonic transducers for transmitting guided waves in rails,” in *Ultrasonics Symposium, 2008. IUS 2008. IEEE*, 2008, pp. 410–413.
5. C. myoung Lee, J. L. Rose, and Y. Cho, “A guided wave approach to defect detection under shelling in rail,” *NDT & E International*, vol. 42, no. 3, pp. 174-180, Apr. 2009.
6. M. J. S. Lowe and O. Diligent, “Low-frequency reflection characteristics of the S0 Lamb wave from a rectangular notch in a plate,” *J. Acoust. Soc. Am.*, vol. 111, no. 1, pp. 64-74, 2002.
7. K. Jezzine and A. Lhémery, “Simulation of guided wave inspection based on the reciprocity principle and the semi-analytical finite element method,” in *Review of*

Progress in Quantitative Nondestructive Evaluation; Volume 26 A(AIP Conference Proceedings Volume 894), 2007, vol. 894, pp. 39–46.

8. Y. N. Al-Nassar, S. K. Datta, and A. H. Shah, "Scattering of Lamb waves by a normal rectangular strip weldment," *Ultrasonics*, vol. 29, pp. 125-132, 1991.
9. F. Benmeddour, F. Treyssède, and L. Laguerre, "Numerical modeling of guided wave interaction with non-axisymmetric cracks in elastic cylinders," *International Journal of Solids and Structures*, vol. 48, no. 5, pp. 764-774, Mar. 2011.
10. M. N. Ichchou, J.-M. Mencik, and W. Zhou, "Wave finite elements for low and mid-frequency description of coupled structures with damage," *Computer Methods in Applied Mechanics and Engineering*, vol. 198, no. 15-16, pp. 1311-1326, Mar. 2009.
11. T. Hayashi, W.-J. Song, and J. L. Rose, "Guided wave dispersion curves for a bar with an arbitrary cross-section, a rod and rail example," *Ultrasonics*, vol. 41, no. 3, pp. 175-183, May. 2003.
12. R. D.Cook, D. S. Malkus, M. E. Plesha and R. J. Witt, "Concepts and Applications of Finite Element Analysis, 4th Edition", John Wiley & Sons, 2002.
13. H. Taweel, S. B. Dong, and M. Kazic, "Wave reflection from the free end of a cylinder with an arbitrary cross-section," *International Journal of Solids and Structures*, vol. 37, no. 12, pp. 1701-1726, Mar. 2000.
14. L. E. Kinsler, A. R. Frey, A. B. Coppens and J. V. Sanders. "Fundamentals of Acoustics", John Wiley & Sons, 1982.